NANO LETTERS

pubs.acs.org/NanoLett

Letter

One-Dimensional Edge Transport in Few-Layer WTe_2

Artem Kononov,* Gulibusitan Abulizi, Kejian Qu, Jiaqiang Yan, David Mandrus, Kenji Watanabe, Takashi Taniguchi, and Christian Schönenberger*

Cite This: *Nano Lett.* 2020, 20, 4228–4233

Read Online

ACCESS | Metrics & More | Article Recommendations | Supporting Information

ABSTRACT: WTe_2 is a layered transitional-metal dichalcogenide (TMD) with a number of intriguing topological properties. Recently, WTe_2 has been predicted to be a higher-order topological insulator (HOTI) with topologically protected hinge states along the edges. The gapless nature of WTe_2 complicates the observation of one-dimensional (1D) topological states in transport due to their small contribution relative to the bulk. Here, we study the behavior of the Josephson effect in magnetic field to distinguish edge from bulk transport. The Josephson effect in few-layer WTe_2 reveals 1D states residing on the edges and steps. Moreover, our data demonstrates a combination of Josephson transport properties observed solely in another HOTI—bismuth, including Josephson transport over micrometer distances, extreme robustness in a magnetic field, and nonsinusoidal current-phase relation (CPR). Our observations strongly suggest the topological origin of the 1D states and that few-layer WTe_2 is a HOTI.

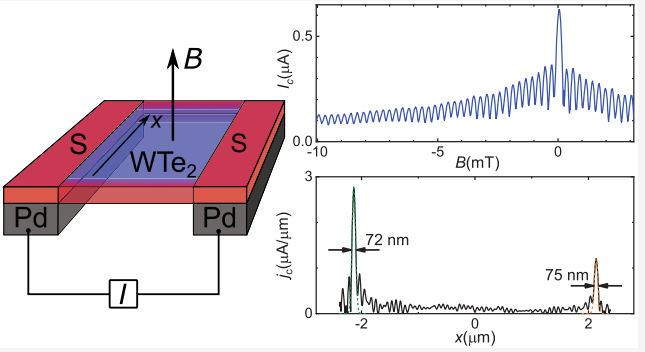

KEYWORDS: *WTe_2, 1D edge states, Josephson effect, nonsinusoidal CPR, higher order topological insulators*

Materials with nontrivial topology attract a lot of attention due to their intriguing properties and the potential to harness them for quantum computing. Nonabelian excitations, occurring when topology meets superconductivity, are especially interesting for applications.[1] Many realizations of these excitations have been proposed and implemented recently, including designing topological superconductivity by combining spin−orbit interaction and Zeeman effect with normal s-wave superconductors,[2] or by proximity inducing superconductivity in topological insulators.[3] Recently, it has also been demonstrated that one can engineer them in hinge states of a higher-order topological insulator (HOTI) combined with proximity induced superconductivity.[4] The layered TMD WTe_2, which in the form of a 3D crystal is a Weyl semimetal[5,6] and a 2D topological insulator in the form of a monolayer,[7,8] has been predicted to be a HOTI,[9] hosting topological hinge states on the edges and steps of the crystal. However, the bulk conductivity of WTe_2 complicates the observation of these states. One way to overcome bulk conductivity is to use local measurement techniques such as scanning tunneling spectroscopy.[4] Another possibility is to employ the Josephson effect.[10−12] Here, the evolution of the critical current $I_c(B_\perp)$ with a perpendicular magnetic field $B_\perp$ is connected with the current distribution in the plane by a Fourier transform.[13] The asymmetry of the critical current can provide additional information about properties of the supercurrent carrying states. The asymmetric Josephson effect (AJE) is expected in systems with a nonsinusoidal CPR,[14] which is often linked with the presence of Andreev bound states with high transmission.[15] The AJE has been previously observed in a 2D topological insulator coupled to a superconductor.[16]

Here, we reveal 1D states along edges and steps in few-layer WTe_2 by studying the Josephson effect in a perpendicular magnetic field. The superconducting contacts required for Josephson junctions are realized by a lithographically patterned Pd film that is in contact with clean WTe_2 and induces superconductivity therein. We found that a Josephson current can be measured over distances up to 3 μm and that it withstands magnetic fields up to 2 T, suggesting its 1D nature with a very tight lateral confinement. Moreover, transport through these 1D states shows signatures of the asymmetric Josephson effect. We think that the observed behavior can be a result of Josephson transport through hinge states due to higher-order topology in WTe_2.

Figure 1(a) demonstrates an optical image of our first device. It consists of a few-layer (∼12) thick WTe_2 flake covered with hBN and placed on the prepatterned Pd leads on

Received: February 14, 2020
Revised: April 19, 2020
Published: May 12, 2020

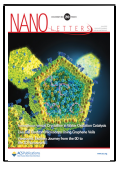

https://dx.doi.org/10.1021/acs.nanolett.0c00658
Nano Lett. 2020, 20, 4228–4233

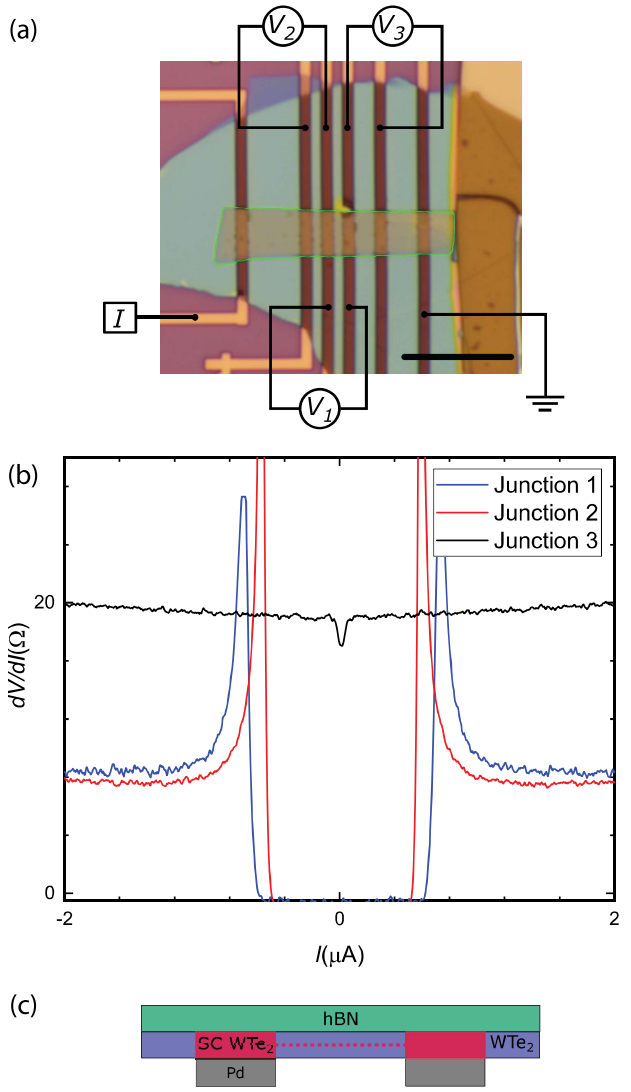

Figure 1. (a) Optical image of the device 1 (scale bar = 10 μm) with a sketch of the four-terminal measurement setup. (b) Four-terminal differential resistances dV/dI of three junctions 1−3 with lengths 1, 1, and 2 μm, respectively. The 1 μm long junctions demonstrate zero differential resistance at small currents as a result of the Josephson effect. (c) Schematic side view of the sample illustrating its state: above the Pd leads WTe_2 is superconducting (red regions), and the current between these regions is mediated by the Josephson effect (dashed lines).

SiO_2 substrate. The leads are forming several junctions with different lengths 1−4 μm. We measured the differential resistances of the junctions in the four-probe setup sketched in Figure 1(a). Additional details of the fabrication process and the measurement setup are provided in the Supporting Information. All measurements were performed in the dilution refrigerator with base temperature of 30 mK.

Figure 1(b) demonstrates experimental dV/dI(I) dependencies of three junctions of the device 1. The differential resistance goes to zero at small currents for the two 1 μm-long junctions. For the 2 μm junction the differential resistance does not go to zero but has a small dip at zero current. Similar results are obtained in all studied samples. Moreover, the observed behavior is present only below a certain temperature and magnetic field. This behavior is typical for Josephson junctions, where the proximity effect creates dissipationless transport between superconductors connected by a normal material.[17] Our experimental data suggest the formation of superconductivity in WTe_2 above Pd leads, as sketched in Figure 1(c). These superconducting regions induce a proximity effect in WTe_2 between the leads, leading to the Josephson effect in the shorter junctions.

The observation of superconductivity may not be surprising, since WTe_2 is known to become superconducting at different conditions, i.e., under pressure,[18,19] electron doping,[20] or electrostatic gating.[21,22] So, superconductivity can occur in WTe_2 on top of Pd due to charge transfer[23] or due to flat-band formation in WTe_2, as has recently been reported in another Weyl semimetal Cd_3As_2.[24] Another possibility is interdifussion of Pd and Te with the formation of superconducting $PdTe_x$[25,26] at the interface. To understand the reasons for superconductivity is beyond the scope of the current article; only the formation of Josephson junction within our samples is important.

We can use the observed Josephson effect to obtain information about the current distribution in the WTe_2 devices. The spatial current distribution defines the evolution of the critical current as a function of the flux through the Josephson junction (JJ). When the supercurrent is uniformly distributed through the JJ, the critical current $I_c(B_\perp)$ as a function of perpendicular magnetic field $B_\perp$ shows oscillations with a rapidly decaying amplitude (top in Figure 2(a)). The central lobe is twice as wide as compared to the other lobes. This dependence of $I_c(B_\perp)$ is known as the Fraunhofer pattern. If, on the other hand, the supercurrent flows only along the sample edges, as indicated in Figure 2(a), $I_c(B_\perp)$ displays slowly decaying oscillations typical for SQUIDs. The period of oscillations corresponds to a single flux quantum $\Phi_0 = h/2e$ through the area enclosed by the SQUID.[17]

Figure 2(b) shows the measured $I_c(B_\perp)$ dependence for the two 1 μm long JJs. The critical current oscillates with perpendicular magnetic field. The central peak of I_c has a width between one and two oscillations periods. The amplitude of the oscillations is decaying faster at smaller fields and slower at larger ones. The measured $I_c(B_\perp)$ is a combination of a Fraunhofer pattern creating a peak of critical current at zero magnetic field and a SQUID-like pattern with more than 50 visible oscillations. The period of these oscillations $\Delta B \sim 0.27$ mT is given by a flux Φ_0 through the effective area of the junction S_{eff}. From S_{eff} we obtain an effective junction length $L_{eff} = S_{eff}/W = 1.75$ μm, where $W \sim 4.3$ μm is the sample width. L_{eff} is larger than the length of the junction L due to the penetration of magnetic field into the superconducting leads. A coexistence of the SQUID and Fraunhofer behavior indicates the precence of edge and bulk supercurrent. The latter can be carried by the bulk of the crystal or by Fermi arc surface states.[27] A persistence of the SQUID-like oscillations in magnetic field means that the edge supercurrent is carried by very narrow states.

To obtain the spatial distribution of the supercurrent, we performed a Fourier transform of $I_c(B_\perp)$ by following the Dynes−Fulton approach.[13] This method assumes a sinusoidal CPR and a nearly symmetric supercurrent distribution across the width of the junction. In this case the minima of $I_c(B)$ should approach zero. The result of the Fourier transform should therefore be more accurate for junction 2 as compared to junction 1, since the $I_c(B)$ minima are found to be much closer to zero in junction 2. Figure 2(c) shows the result of the transformation for junction 2. The supercurrent peaks are very

https://dx.doi.org/10.1021/acs.nanolett.0c00658
Nano Lett. 2020, 20, 4228−4233

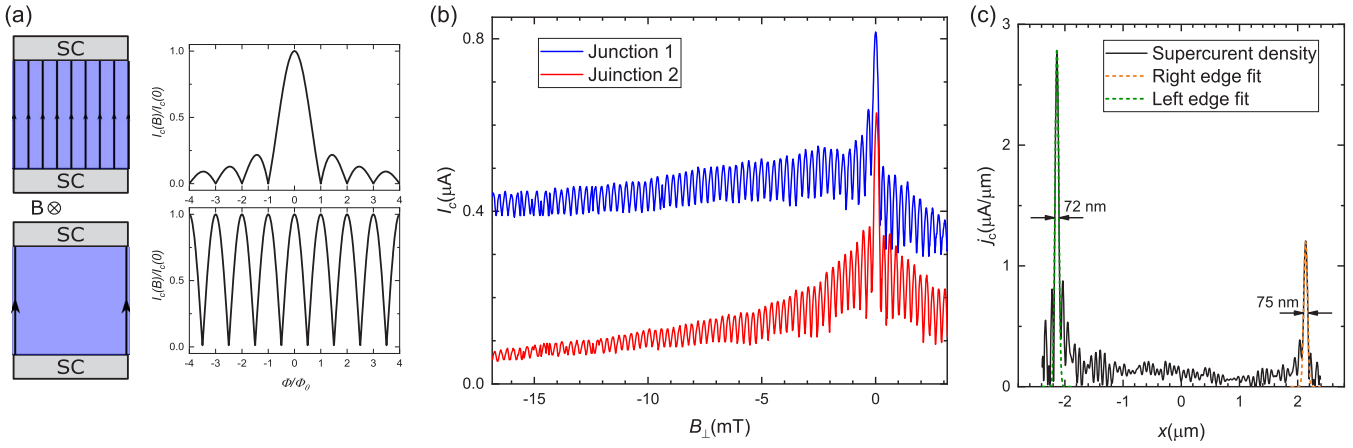

Figure 2. (a) Expected dependencies of the critical current of a 2D Josephson junction on $B_\perp$ for two different supercurrent distributions, i.e., for a uniform current distribution, $I_c(B_\perp)$ shows rapidly decaying oscillations (Fraunhofer behavior), whereas for two narrow edge states, the $I_c(B_\perp)$ oscillations do not (or only weakly) decay in amplitude (SQUID behavior). (b) Critical current $I_c(B_\perp)$ of junctions 1 and 2 as a function of $B_\perp$. A combination of a SQUID- and Fraunhofer-like behavior is observed, indicating a significant amount of edge supercurrent. (c) Supercurrent density distribution of junction 2 extracted from $I_c(B_\perp)$. Two distinctive edge states, each having a width of ∼75 nm, are observed.

narrow, suggesting a strong edge confinement. The width of these supercurrent density peaks obtained from the Gaussian fit is below 80 nm.

There is another reason, beyond an asymmetric current distribution,[13] why the oscillations in Figure 2(b) are not reaching zero; this can be caused by a nonsinusoidal CPR[28,29] of the edge states. We can immediately confirm that the CPR is nonsinusoidal. This is seen as follows. The ratio of the critical currents of the two edge states I_c^H/I_c^L is obtained from the ratio of the average critical current to the critical current oscillation amplitude $I_c^H/I_c^L = (I_c^{max} + I_c^{min})/(I_c^{max} - I_c^{min})$. For junction 1, this ratio is large, $\sim 7 \gg 1$, hence, corresponding to a highly asymmetric SQUID. In such an asymmetric SQUID, the dependence of $I_c(B_\perp)$ on $B_\perp$ mimics directly the CPR of the edge state with the lower critical current.[30] But, $I_c(B)$ for junction 1 is clearly not a sine function, as one can see from Figure 2(b) and Figure 3.

Additional evidence for a nonsinusoidal CPR can be obtained by looking at the symmetry of the dependence $I_c(B_\perp)$ as a function of $B_\perp$. For a conventional Josephson junction with a sinusoidal CPR, $I_c(B_\perp)$ should be symmetrical with respect to current reversal $I_c^+(B_\perp) = I_c^-(B_\perp)$ and magnetic field reversal $I_c(-B_\perp) = I_c(B_\perp)$. Two requirements to break these symmetries are a nonsinusoidal CPR and an asymmetry in the current distribution.[14] However, the time-reversal symmetry conserves I_c upon simultaneous reversal of the magnetic field and the current $I_c^\pm(B_\perp) = I_c^\mp(-B_\perp)$.

As is apparent from Figure 3(a), $I_c^\pm(B_\perp)$ breaks the symmetries both with current and field reversal. The symmetry is restored when the current and magnetic field are reversed simultaneously, as illustrated in Figure 3(b). The time-reversal symmetry allows us to exclude flux trapping in the JJ[31] as a reason for the observed asymmetries. The asymmetries in Figure 3 match the prediction of AJE[14] and require a nonsinusoidal CPR and an asymmetry in current distribution.

We have found before that the supercurrent in few-layer WTe_2 is of 1D nature, flowing predominately along the edges and has a nonsinusoidal CPR. With the next sample we demonstrate that 1D conducting states can also reside at step edges of WTe_2, and they are remarkably robust. Device 2, shown in Figure 4(a), is as before a hBN-covered few-layer

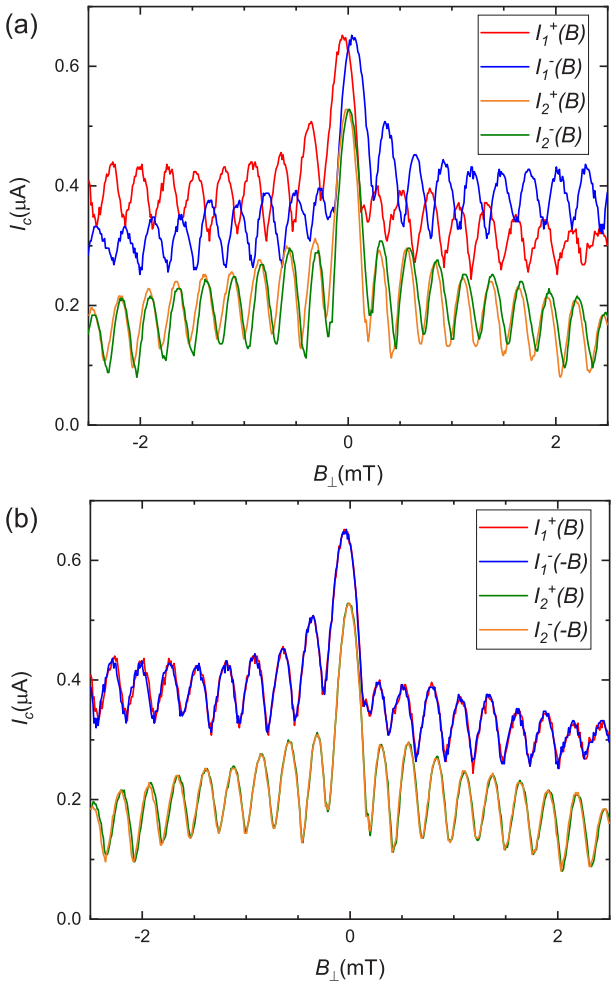

Figure 3. (a) Critical currents of two 1 μm long junctions of device 1 as a function of perpendicular magnetic field for positive $I_{1,2}^+$ and negative $I_{1,2}^-$ currents. $I_c(B_\perp)$ lacks the symmetry to the change of current direction. (b) Same data as in (a) but with a reversed magnetic field for negative currents. Symmetry is preserved when both current and magnetic field are reversed.

https://dx.doi.org/10.1021/acs.nanolett.0c00658
Nano Lett. 2020, 20, 4228−4233

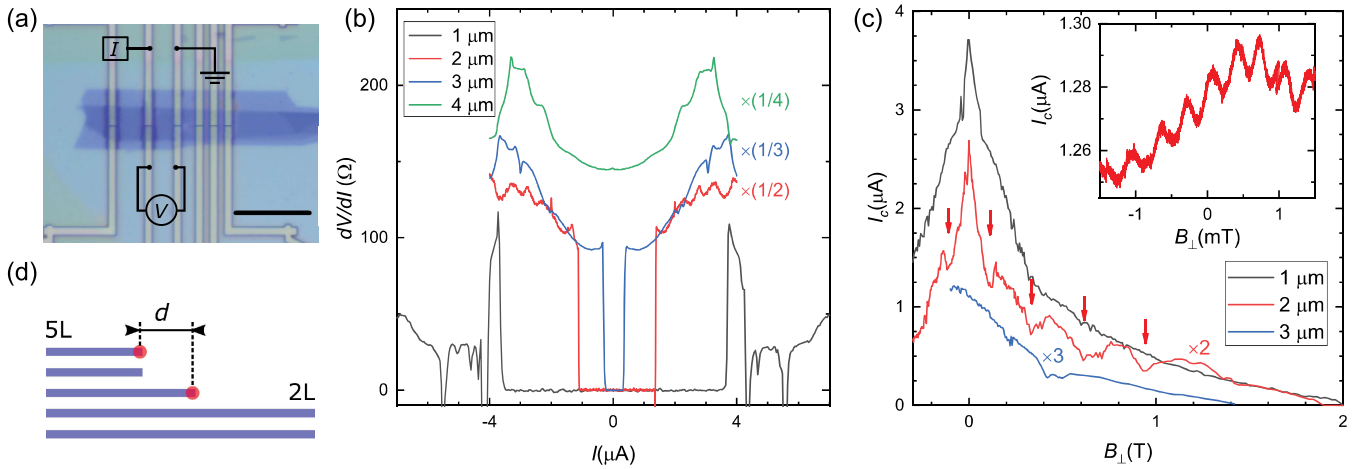

Figure 4. (a) Optical image of device 2 (scale bar = 10 μm) with a sketch of the measurement setup for a single junction. Each Pd lead has a 100 nm gap in the middle, which is located below the thicker part of the WTe_2 flake. The gaps split every Pd lead into two independent normal contacts to the common superconducting region. (b) Four-terminal dV/dI of junctions with different lengths divided by the length of the corresponding junctions in micrometers. The Josephson effect is present in junctions that are up to 3 μm long. (c) Critical current $I_c(B_\perp)$ as a function of perpendicular magnetic field $B_\perp$ (note: I_c is here multiplied by the length of the corresponding junctions in micrometers). The arrows highlight the periodic low-frequency modulation of I_c for the 2 μm long junction. Inset: $I_c(B_\perp)$ for the 2 μm long junction zoomed in to the small magnetic field region. A fast periodic oscillation with an amplitude of ~1% is clearly discerned. (d) Sketch of a cross section of the sample near the step from 5L to 2L, illustrating the possibility that multiple 1D channels along the step appear.

WTe_2 flake placed on top of Pd leads. The main difference from the previous device is nonuniform thickness, where the middle part is five layers thick and the outer parts are bilayers. The low temperature conductivity in WTe_2 diminishes with decrease in number of layers with the bilayer being an insulator.[7,32]

Figure 4(b) shows dV/d$I(I)$ traces for different junctions normalized by the length of the junction. The differential resistance goes to zero for 1−3 μm long junctions, indicating the presence of Josephson current. The normal state resistance per unit length is comparable for all junctions, yielding ~100 Ω μm^{-1}. For this sample, the product I_cR_N ~ 150−380 μV, depending on the junction and the way the normal state resistance R_N is defined. This value is close to the theoretical prediction for a short ballistic Josephson junction: $I_cR_N = \pi\Delta/e$ ~ 540 μV.[33] Here, we estimate the energy gap following the formula $\Delta(T = 0) = 1.76k_BT_c$[17] with T_c = 1.1 K defined as the maximal temperature where signs of superconductivity in the samples are still present. The agreement between the I_cR_N product and the theoretical value implies that there is a strong proximity effect and the JJs are close to the short ballistic limit.

The Josephson current for all junctions survives magnetic fields above 1 T, see Figure 4(c). This is inconsistent with a uniform supercurrent, since even for the shortest junction it would correspond to BS/Φ_0 ~ 2000 flux quantum through the JJ area. A robust large field supercurrent implies highly localized 1D channels that carry the supercurrent. The only possible place for these states are the steps from the five-layer part to bilayers, since the bilayer itself does not conduct. At a closer look, oscillations of $I_c(B_\perp)$ are visible for the 2 μm long junction, see the inset to Figure 4(c). The oscillations are clearly of a SQUID character with a period ΔB ~ 0.33 mT. This period yields a smaller area $S = \Phi_0/\Delta B$ ~ 6.1 μm^2 than the relevant junction's area of 9 μm^2. This mismatch is likely a consequence of the sample geometry and discussed in more detail in the Supporting Information.

The measurement of $I_c(B_\perp)$ of the 2 μm long junction shows additional oscillations with a larger period of δB ~ 0.3 T (red arrows in Figure 4(c)). Similar oscillations were previously observed for topological hinge states in bismuth and were linked to a difference in wavevectors of electrons and holes forming the Andreev pairs.[34] The observed period of oscillations is in agreement with the expected value $\delta B \sim 2\pi\hbar v_F/g_{eff}\mu_B L$ ~ 0.15−0.7 T, where L = 2 μm is the length of the junction, $v_F \sim 2 \times 10^5$ ms^{-1}[35] the Fermi velocity, and g_{eff} ~ 10−50[36] the Landé g-factor. Alternatively, a slower oscillation could reflect the presence of multiple states on terraces from the five layers to the bilayer, as illustrated in Figure 4(d). The width d of this region can be estimated from the ratio of the periods of the slow δB ~ 0.3 T and fast oscillations ΔB ~ 0.33 mT and the width of the junction W ~ 4.5 μm, where $d \sim W\delta B/\Delta B$ ~ 5 nm. This value is an upper estimate for the width of the edge states.

The observation of strong Josephson coupling through 1D edge states with nonsinusoidal CPR suggests a topological origin of these states.[15] The only predicted 1D topological states in few-layer WTe_2 are hinge states of a HOTI.[9] We think that this is very plausible, since our data reproduces many features previously observed in bismuth, which is a HOTI.[10] However, there are still some open questions. Currently we cannot resolve if the states are indeed residing on opposite hinges as expected in a HOTI. Also, the critical current values are higher than expected for a single ballistic channel $I_c^{1D} = \pi\Delta/eR_k = e\Delta/2\hbar$ ~ 20 nA. This discrepancy is also present in bismuth and can be accounted by multiple states at several terraces on the edges and degeneracy of edge states due to multiple orbitals.[10]

In conclusion, we present an experimental study of Josephson transport in encapsulated few-layer WTe_2 samples. Our data strongly suggest the presence of 1D states residing on steps and edges of WTe_2. The Josephson currents in these 1D states are extremely robust. They survive magnetic fields up to 2 T and extend over distances up to 3 μm. Moreover, the supercurrent demonstrates signs of nonsinusoidal CPR. Our findings fit well with the recent prediction of higher-order topological insulator states in WTe_2[9] and demonstrate many

https://dx.doi.org/10.1021/acs.nanolett.0c00658
Nano Lett. 2020, 20, 4228−4233

features previously observed only in another HOTI, i.e., bismuth.[10,34]

Note. During the preparation of this manuscript we became aware of two recent preprints[37,38] demonstrating edge transport in WTe_2 obtained by the proximity effect from superconducting Nb leads. The experimental results in these preprints are in good agreement with our conclusions. In comparison to the former, our samples are in the thin limit and they additionally demonstrate a stronger Josephson coupling over longer distances. They thereby provide a more compelling evidence for Josephson coupling through highly localized narrow 1D states residing on the steps of WTe_2.

■ ASSOCIATED CONTENT

Supporting Information

The Supporting Information is available free of charge at https://pubs.acs.org/doi/10.1021/acs.nanolett.0c00658.

Methods; superconductivity induced in WTe_2 by normal leads; superconductivity and Josephson effect in a few-layer WTe_2 device in a Hall bar geometry; supercurrent distribution in the device 2; and differential resistance as a function of magnetic field and current for the device 2 (PDF)

Accession Codes

All data in this publication are available in numerical form in the Zenodo repository at 10.5281/zenodo.3526560.

■ AUTHOR INFORMATION

Corresponding Authors

Artem Kononov − *Department of Physics, University of Basel, CH-4056 Basel, Switzerland; Institute of Solid State Physics of the Russian Academy of Sciences - Chernogolovka, Chernogolovka 142432, Russia;* orcid.org/0000-0002-3778-8239; Email: Artem.Kononov@unibas.ch

Christian Schönenberger − *Department of Physics and Swiss Nanoscience Institute, University of Basel, CH-4056 Basel, Switzerland;* orcid.org/0000-0002-5652-460X; Email: Christian.Schoenenberger@unibas.ch

Authors

Gulibusitan Abulizi − *Department of Physics, University of Basel, CH-4056 Basel, Switzerland*

Kejian Qu − *Department of Materials Science and Engineering, University of Tennessee, Knoxville, Tennessee 37996, United States*

Jiaqiang Yan − *Materials Science and Technology Division, Oak Ridge National Laboratory, Oak Ridge, Tennessee 37831, United States; Department of Materials Science and Engineering, University of Tennessee, Knoxville, Tennessee 37996, United States;* orcid.org/0000-0001-6625-4706

David Mandrus − *Department of Materials Science and Engineering, University of Tennessee, Knoxville, Tennessee 37996, United States; Materials Science and Technology Division, Oak Ridge National Laboratory, Oak Ridge, Tennessee 37831, United States*

Kenji Watanabe − *National Institute for Material Science, Tsukuba 305-0044, Japan;* orcid.org/0000-0003-3701-8119

Takashi Taniguchi − *National Institute for Material Science, Tsukuba 305-0044, Japan;* orcid.org/0000-0002-1467-3105

Complete contact information is available at: https://pubs.acs.org/10.1021/acs.nanolett.0c00658

Author Contributions

A.K. fabricated the devices 1 and 2, performed the measurements, and analyzed the data. G.A. optimized the fabrication recipe, developed the thickness determination method by optical contrast, and together with A.K. fabricated and measured device S1. K.Q., J.Y., and D.M. provided WTe_2 crystals. K.W. and T.T. provided hBN crystals. A.K prepared the manuscript. C.S. initiated and supervised the project and participated in all discussions. All authors contributed to the manuscript.

Notes

The authors declare no competing financial interest.

■ ACKNOWLEDGMENTS

We thank D. Indolese for the help with measurements of the critical current and fruitful discussions, M. Endres for his help with the exfoliation and identification of WTe_2 flakes, M. Joodaki for her contribution to the optical identification of WTe_2 flakes thickness, and A. Baumgartner for fruitful discussions. A.K. was supported by the Georg H. Endress foundation. This project has received further funding from the European Research Council (ERC) under the European Union's Horizon 2020 research and innovation programme (grant agreement no. 787414 TopSupra), from the Swiss National Science Foundation through the National Centre of Competence in Research Quantum Science and Technology (QSIT), and from the Swiss Nanoscience Institute (SNI). K.W. and T.T. acknowledge support from the Elemental Strategy Initiative conducted by MEXT, Japan, and CREST (JPMJCR15F3), JST. D.M. and J.Y. acknowledge support from the U.S. Department of Energy (U.S. DOE), Office of Science, Basic Energy Sciences (BES), Materials Sciences and Engineering Division.

■ REFERENCES

(1) Nayak, C.; Simon, S. H.; Stern, A.; Freedman, M.; Das Sarma, S. Non-Abelian anyons and topological quantum computation. *Rev. Mod. Phys.* **2008**, *80*, 1083.

(2) Kitaev, A.Yu. Unpaired Majorana fermions in quantum wires. *Phys.-Usp.* **2001**, *44*, 131.

(3) Fu, L.; Kane, C. L. Superconducting Proximity Effect and Majorana Fermions at the Surface of a Topological Insulator. *Phys. Rev. Lett.* **2008**, *100*, 096407.

(4) Jäck, B.; et al. Observation of a Majorana zero mode in a topologically protected edge channel. *Science* **2019**, *364*, 1255.

(5) Soluyanov, A. A.; et al. Type-II Weyl semimetals. *Nature* **2015**, *527*, 495−498.

(6) Li, P.; Wen, Y.; He, X.; Zhang, Q.; Xia, C.; Yu, Z.-M.; Yang, S. A.; Zhu, Z.; Alshareef, H. N.; Zhang, X.-X.; et al. Evidence for topological type-II Weyl semimetal WTe_2. *Nat. Commun.* **2017**, *8*, 2150.

(7) Fei, Z.; et al. Edge conduction in monolayer WTe_2. *Nat. Phys.* **2017**, *13*, 677.

(8) Wu, S.; Fatemi, V.; Gibson, Q. D.; Watanabe, K.; Taniguchi, T.; Cava, R. J.; Jarillo-Herrero, P. Observation of the quantum spin Hall effect up to 100 K in a monolayer crystal. *Science* **2018**, *359*, 76−79.

(9) Wang, Z.; Wieder, B. J.; Li, J.; Yan, B.; Bernevig, B. A. Higher-Order Topology, Monopole Nodal Lines, and the Origin of Large Fermi Arcs in Transition Metal Dichalcogenides XTe_2 (X = Mo,W). *Phys. Rev. Lett.* **2019**, *123*, 186401.

(10) Murani, A.; Kasumov, A.; Sengupta, S.; Kasumov, Y. A.; Volkov, V. T.; Khodos, I. I.; Brisset, F.; Delagrange, R.; Chepelianskii, A.; Deblock, R.; Bouchiat, H.; Gueron, S. Ballistic edge states in

Bismuth nanowires revealed by SQUID interferometry. *Nat. Commun.* **2017**, *8*, 15941.
(11) Schindler, F.; et al. Higher-order topology in bismuth. *Nat. Phys.* **2018**, *14*, 918.
(12) Shvetsov, O. O.; Kononov, A.; Timonina, A. V.; Kolesnikov, N. N.; Deviatov, E. V. Realization of a Double-Slit SQUID Geometry by Fermi Arc Surface States in a WTe_2 Weyl Semimetal. *JETP Lett.* **2018**, *107*, 774.
(13) Dynes, R. C.; Fulton, T. A. Supercurrent density distribution in Josephson Junctions. *Phys. Rev. B* **1971**, *3*, 3015.
(14) Chen, C.-Z.; He, J. J.; Ali, M. N.; Lee, G. H.; Fong, K. C.; Law, K. T. Asymmetric Josephson effect in inversion symmetry breaking topological materials. *Phys. Rev. B: Condens. Matter Mater. Phys.* **2018**, *98*, 075430.
(15) Sochnikov, I.; Maier, L.; Watson, C. A.; Kirtley, J. R.; Gould, C.; Tkachov, G.; Hankiewicz, E. M.; Brüne, C.; Buhmann, H.; Molenkamp, L. W.; Moler, K. A. Nonsinusoidal Current-Phase Relationship in Josephson Junctions from the 3D Topological Insulator HgTe. *Phys. Rev. Lett.* **2015**, *114*, 066801.
(16) Bocquillon, E.; et al. Gapless Andreev bound states in the quantum spin Hall insulator HgTe. *Nat. Nanotechnol.* **2017**, *12*, 137.
(17) Tinkham, M. *Introduction to Superconductivity*, 2nd ed.; McGraw-Hill, Inc.: New York, 1996.
(18) Kang, D.; et al. Superconductivity emerging from a suppressed large magnetoresistant state in tungsten ditelluride. *Nat. Commun.* **2015**, *6*, 7804.
(19) Pan, X.-C.; et al. Pressure-driven dome-shaped superconductivity and electronic structural evolution in tungsten ditelluride. *Nat. Commun.* **2015**, *6*, 7805.
(20) Asaba, T.; Wang, Y.; Li, G.; Xiang, Z.; Tinsman, C.; Chen, L.; Zhou, S.; Zhao, S.; Laleyan, D.; Li, Y.; Mi, Z.; Li, L. Magnetic Field Enhanced Superconductivity in Epitaxial Thin Film WTe_2. *Sci. Rep.* **2018**, *8*, 6520.
(21) Sajadi, E.; et al. Gate-induced superconductivity in a monolayer topological insulator. *Science* **2018**, *362*, 922.
(22) Fatemi, V.; et al. Electrically tunable low-density superconductivity in a monolayer topological insulator. *Science* **2018**, *362*, 926.
(23) Shao, B.; Eich, A.; Sanders, C.; Ngankeu, A. S.; Bianchi, M.; Hofmann, P.; Khajetoorians, A. A.; Wehling, T. O. Pseudodoping of a metallic two-dimensional material by the supporting substrate. *Nat. Commun.* **2019**, *10*, 180.
(24) Shvetsov, O. O.; Esin, V. D.; Timonina, A. V.; Kolesnikov, N. N.; Deviatov, E. V. Surface superconductivity in three-dimensional Cd_3As_2 semimetal at the interface with a gold contact. *Phys. Rev. B: Condens. Matter Mater. Phys.* **2019**, *99*, 125305.
(25) Tiwari, B.; Goyal, R.; Jha, R.; Dixit, A.; Awana, V. P. S. PdTe: a 4.5 K type-II BCS superconductor. *Supercond. Sci. Technol.* **2015**, *28*, 055008.
(26) Teknowijoyo, S.; et al. Nodeless superconductivity in the type-II Dirac semimetal $PdTe_2$: London penetration depth and pairing-symmetry analysis. *Phys. Rev. B: Condens. Matter Mater. Phys.* **2018**, *98*, 024508.
(27) Kononov, A.; et al. Signature of Fermi arc surface states in Andreev reflection at the WTe_2 Weyl semimetal surface. *EPL* **2018**, *122*, 27004.
(28) Kurter, C.; Finck, A. D. K.; Hor, Y. S.; Van Harlingen, D. J. Evidence for an anomalous current−phase relation in topological insulator Josephson junctions. *Nat. Commun.* **2015**, *6*, 7130.
(29) Pribiag, V.; Beukman, A.; Qu, F.; et al. Edge-mode superconductivity in a two-dimensional topological insulator. *Nat. Nanotechnol.* **2015**, *10*, 593−597.
(30) Nanda, G.; et al. Current-Phase Relation of Ballistic Graphene Josephson Junctions. *Nano Lett.* **2017**, *17*, 3396.
(31) Golod, T.; Rydh, A.; Krasnov, V. M. Detection of the Phase Shift from a Single Abrikosov Vortex. *Phys. Rev. Lett.* **2010**, *104*, 227003.
(32) Wang, L.; et al. Tuning magnetotransport in a compensated semimetal at the atomic scale. *Nat. Commun.* **2015**, *6*, 8892.
(33) Kulik, I. O.; Omelyanchuk, A. N. Properties of superconducting microbridges in the pure limit. *Fiz. Nizk. Temp. [Sov. J. Low Temp. Phys.]* **1977**, *3* (7), 945.
(34) Li, C.; et al. Magnetic field resistant quantum interferences in Josephson junctions based on bismuth nanowires. *Phys. Rev. B: Condens. Matter Mater. Phys.* **2014**, *90*, 245427.
(35) Huang, C.; et al. Inducing Strong Superconductivity in WTe_2 by a Proximity Effect. *ACS Nano* **2018**, *12*, 7185.
(36) Bi, R.; et al. Spin zero and large Landé *g*-factor in WTe_2. *New J. Phys.* **2018**, *20*, 063026.
(37) Choi, Y.-B.; Xie, Y.; Chen, C.-Z.; Park, J.-H.; Song, S.-B.; Yoon, J.; Kim, B. J.; Taniguchi, T.; Watanabe, K.; Lee, H.-J.; Kim, J.-H.; Fong, K. C.; Ali, M. N.; Law, K. T.; Lee, G.-H. Evidence of Higher Order Topology in Multilayer WTe_2 from Josephson Coupling through Anisotropic Hinge States. *arXiv* (Mesoscale and Nanoscale Physics), September 5, 2019, arXiv:1909.02537; https://arxiv.org/abs/1909.02537 (accessed May 8, 2020).
(38) Huang, C.; Narayan, A.; Zhang, E.; Liu, S.; Yi, C.; Shi, Y.; Sanvito, S.; Xiu, F. Observation of Edge States in Multilayer WTe_2. *arXiv* (Superconductivity), September 5, 2019, arXiv:1909.02433; https://arxiv.org/abs/1909.02433 (accessed May 8, 2020).

https://dx.doi.org/10.1021/acs.nanolett.0c00658
Nano Lett. 2020, 20, 4228−4233